CONCLUSION

These studies suggest:

1. Various enzymes catalyze the hydrolysis of ^{99m}Tc-ECD, and the enzymatic systems are different between tissues and between species.
2. pH has little effect on ^{99m}Tc-ECD metabolism in the brain.
3. There are regional differences in intracranial metabolic activity in cynomolgus monkey.
4. In both rat and cynomolgus monkey tissue, metabolic activity is low in blood, intermediate in brain and high in liver.

It remains to be determined whether regional differences in metabolic activity in the intracranial tissues influence ^{99m}Tc-ECD SPECT images.

REFERENCES

1. Moretti JL, Caglar M, Weinmann P. Cerebral perfusion imaging tracers for SPECT: which one to choose? *J Nucl Med* 1995;36:359–363.
2. Leveille J, Demonceau G, De Roo M, et al. Characterization of technetium-99m-L,L-ECD for brain perfusion imaging, part 2: biodistribution and brain imaging in humans. *J Nucl Med* 1989;30:1902–1920.
3. Walovitch RC, Hill TC, Garrity ST, et al. Characterization of technetium-99m-L,L-ECD for brain perfusion imaging, part 1: pharmacology of technetium-99m ECD in nonhuman primates. *J Nucl Med* 1989;30:1892–1901.
4. Walovitch RC, Franceschi M, Picard M, et al. Metabolism of ^{99m}Tc-L,L-ethyl cysteinate dimer in healthy volunteers. *Neuropharmacology* 1991;30:283–292.
5. Walovitch RC, Cheesman EH, Maheu LJ, Hall KM. Studies of the retention mechanism of the brain perfusion imaging agent, ^{99m}Tc-bicisate (^{99m}Tc-ECD). *J Cereb Blood Flow Metab* 1994;14(suppl 1):S4–S11.
6. Holmes RS, Masters CJ. The developmental multiplicity and isoenzyme status of cavian esterases. *Biochem Biophys Acta* 1967;132:379–399.
7. Bormans G, Van Nerom C, De Beukelaer C, Hoogmartens M, De Roo M, Verbruggen A. Comparison of ^{99m}Tc-ECD metabolism in organ homogenates of rat and baboon [Abstract]. *Eur J Nucl Med* 1989;15:423.
8. Yonekura Y, Nishizawa S, Mukai T, et al. Functional mapping of flow and back-diffusion rate of N-isopropyl-p-iodoamphetamine in human brain. *J Nucl Med* 1993;34:839–844.
9. Kawashima R, Koyama M, Ito H, et al. Normal cerebral perfusion of ^{99m}Tc-ECD brain SPECT: evaluation by an anatomical standardization technique. *Kakuigaku* 1996;33: 69–72.
10. Van Nerom C, Bormans G, De Beukelaer C, De Roo M, Verbruggen A. Metabolism of ^{99m}Tc-ECD in organ homogenates of baboon [Abstract]. *Eur J Nucl Med* 1989;15:423.

Imaging Nicotinic Acetylcholine Receptors with Fluorine-18-FPH, an Epibatidine Analog

Victor L. Villemagne, Andrew Horti, Ursula Scheffel, Hayden T. Ravert, Paige Finley, David J. Clough, Edythe D. London, Henry N. Wagner, Jr. and Robert F. Dannals

Divisions of Nuclear Medicine and Radiation Health Sciences, The Johns Hopkins Medical Institutions; and Brain Imaging Section, Intramural Research Program, National Institute on Drug Abuse, National Institutes of Health, Baltimore, Maryland

Nicotinic acetylcholine receptors (nAChRs) have been implicated in a variety of central processes, such as learning and memory and analgesia. These receptors also mediate the reinforcing properties of nicotine in tobacco products and are increased in postmortem samples of brains of smokers. On the other hand, brains of individuals who have died from dementia of the Alzheimer type show abnormally low densities of nAChRs. In this study, the distribution and kinetics of [(±)-exo-2-(2-[^{18}F] fluoro-5-pyridyl)-7-azabicyclo[2.2.1]heptane (^{18}F-FPH), a high-affinity nAChR agonist, was evaluated in a baboon using PET. **Methods:** After intravenous injection of 5 mCi [185 MBq] ^{18}F-FPH into a 25-kg anesthetized baboon, sequential quantitative tomographic data were acquired over a period of 150 min. Regions of interest were placed and time-activity curves were generated. Brain kinetics of the radiotracer were calculated, and the in vivo regional binding in the baboon brain was compared with the known in vitro regional distribution of nAChRs in the rat and human brain. **Results:** Brain activity reached a plateau within 60 min after injection of the tracer, and the binding was reversible. Elimination of ^{18}F-FPH was relatively rapid from the cerebellum (clearance $t_{1/2}$ = 3 hr), intermediate from the hypothalamus/midbrain ($t_{1/2}$ = 7 hr) and slow from the thalamus ($t_{1/2}$ = 16 hr). Radioactivity due to ^{18}F-FPH at 130 min postinjection was highest in the thalamus and hypothalamus/midbrain, intermediate in the neocortex and hippocampus and lowest in the cerebellum. Subcutaneous injection of 1 mg/kg cytisine 45 min after injection of the radiotracer reduced brain activity at 130 min by 67%, 64%, 56% and 52% of control values in the thalamus, hypothalamus/midbrain, hippocampus and cerebellum, respectively. The regional binding of ^{18}F-FPH at 130 min was highly correlated with the known densities of nAChR measured in vitro in human (r = 0.81) and rat brain (r = 0.90). **Conclusion:** These results demonstrate the feasibility of imaging nAChRs in vivo. Fluorine-18-FPH appears to be a suitable tracer to study nAChRs in the human brain.

Key Words: nicotinic receptors; PET; nonhuman primate; brain; epibatidine

J Nucl Med 1997; 38:1737–1741

Nicotinic acetylcholine receptors (nAChRs) have been implicated in a variety of central processes, such as learning and memory (*1–4*) and antinociception (*5*). These receptors also mediate the reinforcing properties of nicotine in tobacco products (*6,7*). The loss of cholinergic neurons in the basal forebrain has been associated with a variety of pathological disorders, such as senile dementia of the Alzheimer type, Huntington's and Parkinson's diseases and progressive supranuclear palsy (*8–15*).

Neuronal nAChRs are ligand-gated ion channels composed of two kinds of subunits (α and β) (*1*). There are at least three subtypes of nAChRs in the central nervous system as identified by radioligand binding techniques (*1,16*): (a) those with high affinity for (-)-nicotine, which are labeled by agonists such as ^{3}H-acetylcholine and ^{3}H-cytisine (nicotine/ACh) (*17*); (b) those with high affinity for ^{125}I-α-bungarotoxin (αBgT) (*18*); and (c) those that selectively recognize neuronal bungarotoxin (n-BgT) (*19*). The pharmacological profile of a receptor subtype is related to its subunit combination. There is a good correlation between the distribution of nAChRs with the $\alpha4\beta2$ subunit combination and the distribution of high-affinity nicotine/ACh

Received Sep. 12, 1996; revision accepted Dec. 19, 1996.

For correspondence or reprints contact: Robert F. Dannals, PhD, Division of Nuclear Medicine, The Johns Hopkins Medical Institutions, 615 North Wolfe St., Room 2001, Baltimore, MD 21205–2179.

binding sites (*20*), between the distribution of α7 mRNA and αBgT high-affinity binding sites (*18*), and between α3 mRNA and n-BgT binding sites (*19*).

Carbon-11-methyl-(-)-nicotine has been used to study nAChRs in nonhuman primates, normal human volunteers (*21*) and patients with Alzheimer's disease (*22*) by means of PET. However, the high nonspecific binding and rapid clearance of [^{11}C-methyl]-(-)-nicotine from the brain preclude the widespread use of this radioligand in the in vivo evaluation of nAChRs in human subjects.

Epibatidine ((-)-exo-2-(2-chloro-5-pyridyl)−7-azabicyclo [2.2.1]heptane), an extract of frog skin, is a potent alkaloid with antinociceptive properties and extremely high affinity for nAChRs in vitro (*23–25*). In vivo studies with [^{3}H]epibatidine in mice showed high brain uptake of the tracer, a regional distribution consistent with that of nAChRs, a slow clearance from brain and low estimates of nonspecific binding (*26*). The in vivo biodistribution of the [^{3}H]norchloro analog was similar to that of the parent compound (*27*).

In this study, an in vivo characterization of the distribution and kinetics of (±)-exo-(2-[^{18}F]fluoro-5-pyridyl)−7-azabicyclo[2.2.1]heptane (^{18}F-FPH) (*28*) binding to nAChRs in the baboon brain was performed using PET. To demonstrate specific binding to nAChRs receptors, the regional distribution and specificity of the binding were examined.

MATERIALS AND METHODS

For the PET procedures, a 25-kg male baboon (Papio Anubis) was initially anesthetized with 8–10 mg/kg alfadolone and alfaxolone acetate (Saffan®) intramuscularly and intubated. Anesthesia was maintained throughout the study by a continuous intravenous infusion drip of 6–9 mg/kg/h alfadolone and alfaxolone acetate.

The baboon was then comfortably restrained to the PET bed using an individually fitted thermoplastic mask that allowed reproducible positioning between studies. Pulse and oxygen saturation were continuously monitored during the studies. Blood oxygen saturation was always maintained above 85%.

No-carrier-added (±)-exo-2-(2-[^{18}F]fluoro-5-pyridyl)−7-azabicyclo[2.2.1]heptane (^{18}F-FPH) and authentic (±)-exo-2-(2-fluoro-5-pyridyl)−7-azabicyclo[2.2.1]heptane (FPH) were prepared as previously described (*28*). Briefly, a solution of (±)-exo-2-(2-bromo-5-pyridyl)−7-azabicyclo[2.2.1]heptane in DMSO was stirred with K (*18*)F/Kryptofix 222® complex for 15 min at 200°C. The labeled product was purified by preparative high-performance liquid chromatography. Chemical and radiochemical purities, determined by HPLC, exceeded 95%. Sterility and apyrogenicity testing were performed using standard procedures. The average specific activity of the final product calculated at the end of synthesis was greater than 2000 mCi/μmol. Authentic, unlabeled FPH, used as a standard in HPLC, was prepared by Kryptofix®222-assisted nucleophilic fluorination of (±)-exo-2-(2-bromo-5-pyridyl)−7-methoxycarbonyl-7-azabicyclo[2.2.1]heptane followed by acid deprotection.

After the baboon was positioned in the PET scanner, a transmission scan was performed with a ^{68}Ga source to allow for attenuation correction. PET scanning was started immediately after intravenous injection of 5 mCi [185 MBq] of high specific activity ^{18}F-FPH (corresponding to 0.12 nmol/kg); 15 simultaneous (eight direct planes, seven cross planes, Z axis = ~10 cm) sequential quantitative tomographic slices of the brain were obtained with the GE 4096+ PET tomograph in the high-resolution mode (~6.5 mm FWHM) over a period of 150 min. The baboon was positioned so that the lowest plane was located about 5 cm below the canthomeatal line. No blood samples to measure plasma radioactivity were obtained. In a second study measuring displacement of

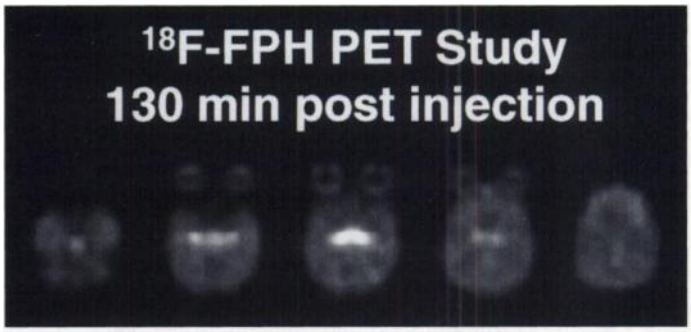

FIGURE 1. Black and white coded transforms of PET scans showing ^{18}F-FPH binding in the baboon brain at 130 mpi. There is high uptake of the radiotracer in the thalamus and hypothalamus/midbrain regions, intermediate uptake in the frontal cortex and low uptake in the cerebellum.

^{18}F-FPH from nAChRs, 1 mg/kg of cytisine, a selective partial agonist at nAChRs (*1*), was injected intravenously 45 min after administration of the radiotracer.

PET images were reconstructed from the raw data with a standard filtered backprojection algorithm and a Hann filter (6.0 mm). Images were also corrected for attenuation and decay and normalized for injected dose. Regions of interest were manually placed over the different areas of the baboon brain with reference to a baboon PET atlas (*29*), and time-activity curves were generated.

Brain kinetics of the radiotracer were calculated by fitting all the regional radioactivity concentration values at the different time points to a triple exponential equation:

$$E_{(t)} = Ae^{-\alpha t} + Be^{-\beta t} + Ce^{-\lambda t}$$

where E is the brain radioactivity concentration and A, B and C are coefficients for the initial rapid distribution (α), distribution/disposition (β), and elimination (λ) phases, respectively, with the constraint $E_{(0)} = 0$. The clearance $t_{1/2}$ was calculated as: $t_{1/2} = 0.693/\lambda$. The time/activity data were fit using a nonlinear regression program, MacCurveFit (Kevin Raner Software, Inc., Mt. Waverley, Victoria, Australia), run on a Macintosh personal computer.

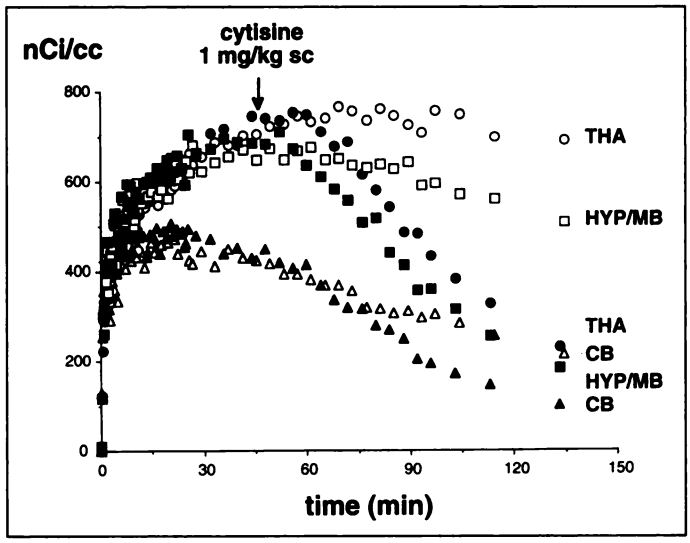

FIGURE 2. Time-activity curves from the thalamus (THA), hypothalamus/midbrain (HYP/MD) and cerebellum (CB). Note that in the control study (open symbols THA ○, HYP/MD □, CB △) the radioactivity reaches a plateau around 50 min after radiotracer injection followed by a slow dissociation. The administration of 1 mg/kg cytisine at 45 min after tracer injection (full symbols THA ●, HYP/MD ■, CB ▲) markedly decreased the ^{18}F-FPH binding in all areas, showing specificity of the binding of ^{18}F-FPH to nAChRs.

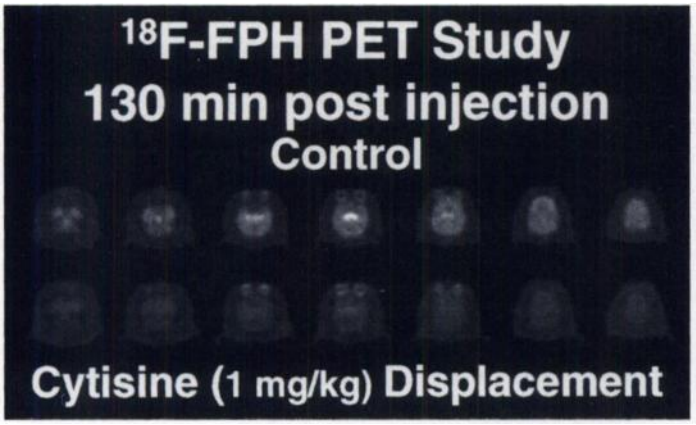

FIGURE 3. Black and white coded transforms of PET scans showing ^{18}F-FPH binding to the baboon brain at 130 mpi in the control study (upper row) and after displacement with 1 mg/kg cytisine (lower row). There is a decrease of binding in all brain areas, but there is no decrease in the activity in the eyes.

The in vivo regional binding in the baboon brain was compared with the known in vitro regional distribution of nAChRs labeled with ^{3}H-nicotine (*30*), ^{3}H-cytisine and ^{3}H-epibatidine (*25*) in the rat brain and ^{3}H-nicotine in human brain (*31*).

RESULTS

Radioactivity was distributed heterogeneously in the brain. Cortical, subcortical and cerebellar structures were well identified (Fig. 1). Brain radioactivity reached a plateau approximately at 60 min postinjection, and the binding was reversible (Fig. 2). Elimination was relatively rapid from the cerebellum (clearance $t_{1/2}$ = 3 hr), intermediate from the hypothalamus/midbrain ($t_{1/2}$ = 7 hr) and slow from the thalamus ($t_{1/2}$ = 16 hr). Radioactivity due to ^{18}F-FPH at 130 min postinjection was highest in the thalamus and hypothalamus/midbrain, intermediate in the neocortex and hippocampus and lowest in the cerebellum.

Subcutaneous injection of 1 mg/kg cytisine 45 min after the injection of the radiotracer reduced brain radioactivity at 130 min by 67%, 64%, 56% and 52% of control values in the thalamus, hypothalamus/midbrain, hippocampus and cerebellum, respectively (Fig. 3), indicating that the binding of ^{18}F-FPH to nAChRs is specific. There was no change in the radioactivity observed in the eyes after injection of cytisine (Fig. 3).

Binding of ^{18}F-FPH at 130 min was highly correlated with the known densities of nAChR measured in vitro by ^{3}H-nicotine (r = 0.97), ^{3}H-cytisine (r = 0.97), ^{3}H-epibatidine (r = 0.91) in rat brain and by ^{3}H-nicotine in human brain (r = 0.81) (Fig. 4); in other words, high in the thalamus, intermediate in the hippocampus and low in cerebellum (*25,30,31*).

DISCUSSION

Epibatidine is reported to be the ligand with the highest affinity for nAChRs in vitro ($K_i \sim 50$ p*M*) (*23*). An analog of epibatidine, FPH fumarate, competitively displaced ^{3}H-epibatidine in in vitro binding studies with K_i values of 45 p*M* (*32*). In this study the kinetics and brain regional distribution of a fluorinated analog of epibatidine, ^{18}F-FPH, were successfully examined using PET. Although FPH produces toxicity in mice

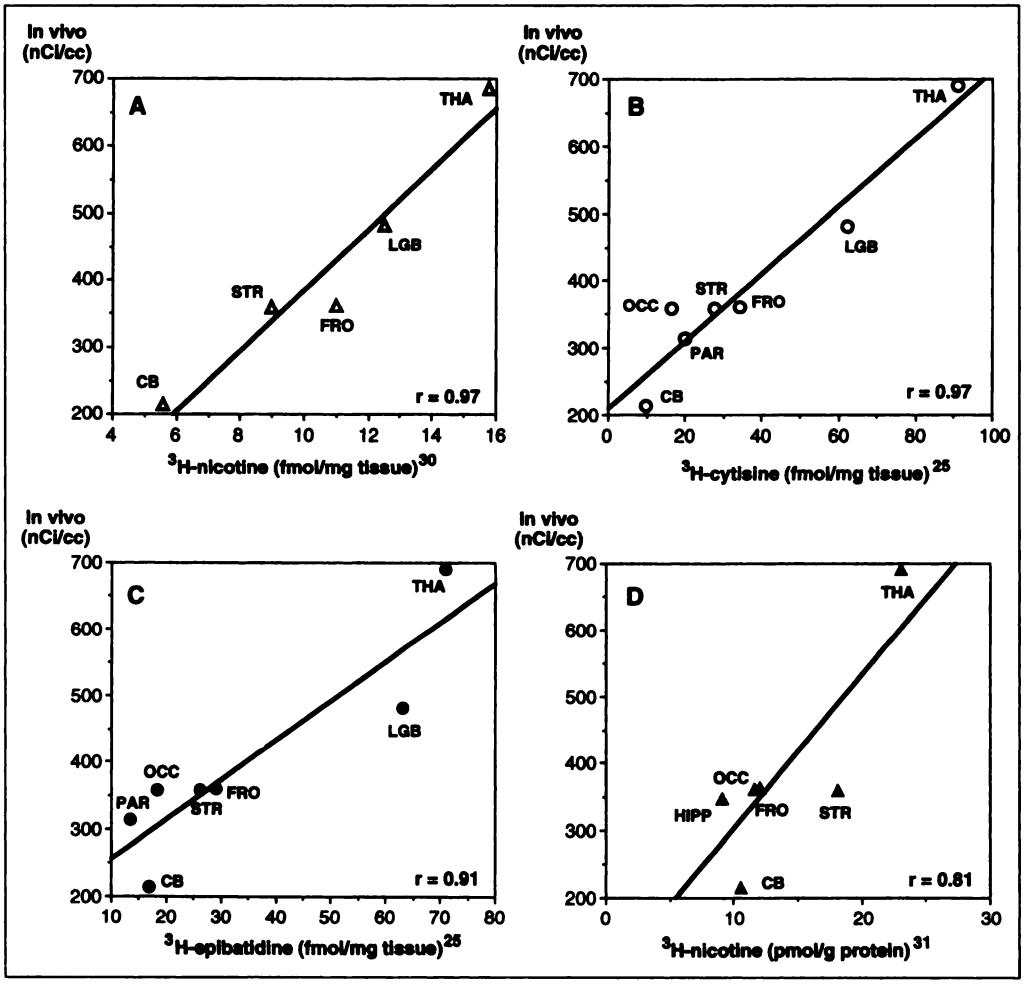

FIGURE 4. The in vivo regional distribution in the baboon is compared to the known in vitro regional distribution of nAChRs in the (A, B, C) rat and (D) human brains. THA = thalamus, LGB = lateral geniculate body, STR = striatum, HIPP = hippocampus, FRO = frontal cortex, OCC = occipital cortex, PAR = parietal cortex and CB = cerebellum.

(LD50 ~ 40 nmol/kg) (Scheffel, *personal communication*, 1996), injection of the 5 mCi [185 MBq] dose of high specific activity ^{18}F-FPH (0.12 nmol/kg) did not cause a change in either blood pressure or heart rate.

Although radioactivity was lowest in the cerebellum, there is no region of the brain completely devoid of nAChRs that is large enough to be sampled by PET. There are species differences in the distribution of nAChRs in the mammalian brain. Binding of ^{3}H-nicotine in the human brain is highest in the thalamus and striatum, intermediate in the hypothalamus and neocortex and lowest in the hippocampus and pons (*31*). In contrast, ^{3}H-nicotine binding is low in the monkey striatum compared to the thalamus (*33*), while it is high in the neocortex of the rat (*18,30*) and the mouse (*34*). A baboon was chosen for this study because this is a species close to humans and, therefore, the possibility of significant species differences in the biodistribution is reduced. In addition, the relatively large size of the baboon brain makes it suitable for PET imaging.

Fluorine-18-FPH binding to nAChRs exhibits pharmacological specificity. Cytisine, a nicotine partial agonist, has high affinity for the nicotine/ACh receptor subtype (*17*). Previous studies using in vitro binding assay techniques, as well as functional assays, found that in the rodent brain both epibatidine and cytisine are bound to the nicotine/ACh subtype, mainly composed of $\alpha4\beta2$ subunits (*1*). In vitro studies have shown that (±)-epibatidine competitively displaced ^{3}H-cytisine from $\alpha4\beta2$ nAChRs subtypes in the rat brain in a concentration-dependent fashion consistent with a single-site competitive model with K_i values of 43 p*M* (*35*). After the administration of cytisine, marked decreases in ^{18}F-FPH binding were observed in regions of the brain known to contain high concentrations of the nicotine/ACh receptor subtype. Administration of cytisine had no effect on ^{18}F-FPH binding in the region of the eyes, where the n-BgT receptor subtype abounds (*36*). Similar findings in the visual system were reported using ^{3}H-epibatidine in rats (*24,25*). Our results provide further evidence that ^{18}F-FPH binds to nAChR subtypes other than the nicotine/ACh subtype.

The in vivo regional distribution of ^{18}F-FPH is consistent with the regional distribution of ^{3}H-nicotine and ^{3}H-cytisine binding sites examined by in vitro methods in postmortem human, monkey and rat brains (*25,30,31,33*). Persistence of FPH binding in the eyes after administration of cytisine also is consistent with the known distribution of the n-BgT receptor subtype (*36*).

Collection of arterial plasma, and identification of metabolites in plasma, would be needed to further characterize the binding of FPH in a quantitative fashion. Based on previous mouse data (*32*) and in our preliminary results, we think that longer scanning protocols would allow for equilibrium to be achieved. The advantage of studying receptors with a PET radiotracer labeled with a radioisotope such as ^{18}F ($T_{1/2}$ = 109 min) is that it allows for extended scanning after injection, which increases the contrast between regions of high- and low-receptor density, permitting attainment of steady state during the scanning period, thus facilitating quantification of the binding potential, such as applied to other reversible binding ligands (*37*). However, this approach might not be feasible because there is no region completely devoid of receptors that can be used as a reference region. If equilibrium is not achieved, and due to the toxicity of epibatidine that precludes studies with low specific activity as proposed by Huang et al. (*38*), full kinetic compartmental analysis varying the available number of binding sites by a competing drug, such as cytisine, as proposed by Wong et al. (*39,40*), or a simplified approach using the Gjedde-Patlak (*41,42*) linear transformation, could be applied. Further studies to address these issues are warranted.

CONCLUSION

The results obtained in this study demonstrate the feasibility of nAChRs imaging in vivo with PET and suggest that ^{18}F-FPH is potentially useful to study the physiologic role and the pathological states of nAChRs in the human brain.

ACKNOWLEDGMENTS

The authors thank Karen Edmons for her assistance with PET data acquisition and Robert Smoot for technical assistance with cyclotron operation and radiochemistry. This work was supported in part by U.S. Public Health Service grant # CA 32845, the Division of Intramural Research, National Institute on Drug Abuse (NIDA), and funding for the NIDA Brain Imaging Facility from the Counterdrug Technology Assessment Center, Office of National Drug Control Policy.

REFERENCES

1. Decker MW, Brioni JD, Bannon AW, Arneric SP. Diversity of neuronal nicotinic acetylcholine receptors: lessons from behavior and implications for CNS therapeutics. *Life Sci* 1995;56:545–570.
2. Flicker DRL, Watkins DL, Fisher SK, Bartus RT. Behavioral and neurochemical effects following neurotoxic lesions of a major cholinergic input to cerebral cortex in rat. *Pharmacol, Biochem and Behav* 1983;18:973–981.
3. Irle E, Markowitsch HJ. Basal forebrain-lesioned monkeys are severely impaired in tasks of association and recognition memory. *Ann Neurol* 1985;14:1025–1032.
4. Levin ED, Rose JE. Acute and chronic nicotinic interactions with dopamine systems and working memory performance. *Ann N Y Acad Sci* 1995;757:245–252.
5. Pert A. Cholinergic and catecholaminergic modulation of nociceptive reactions. Interactions with opiates. In: Akil H, Lewis JW, eds. *Pain and headache, neurotransmitters and pain control.* Basel, Switzerland: S Karger; 1987:1–63
6. Benowitz NL, Porchet H, Jacob P III. Nicotine dependence and tolerance in man: pharmacokinetic and pharmacodynamic investigations. *Prog Brain Res* 1989;79:279–287.
7. Henningfield JE, Woodson PP. Dose-related actions of nicotine on behavior and physiology: review and implications for replacement therapy for nicotine dependence. *J Subst Abuse* 1989;1:301–317.
8. Araujo DM, Lapchak PA, Robitaille Y, Gauthier S, Quirion RJ. Differential alteration of various cholinergic markers in cortical and subcortical regions of human brain in Alzheimer's disease. *Neurochem* 1988;50:1914–1923.
9. Kellar KJ, Whitehouse PJ, Martino-Barrows AM, Marcus K, Price DL. Muscarinic and nicotinic cholinergic binding sites in Alzheimer's disease cerebral cortex. *Brain Res* 1987;436:62–68.
10. London ED, Ball MJ, Waller SB. Nicotinic binding sites in cerebral cortex and hippocampus in Alzheimer's dementia. *Neurochem Res* 1989;14:745–750.
11. Nordberg A, Winblad B. Reduced number of [^{3}H]nicotine and [^{3}H]acetylcholine binding sites in the frontal cortex of Alzheimer brains. *Neurosci Lett* 1986;72:115–119.
12. Palacios JM, Mengod G, Vilaro MT, et al. Cholinergic receptors in the rat and human brain: microscopic visualization. *Prog Brain Res* 1990;84:243–253.
13. Whitehouse PJ, Martino AM, Antuono PG, Lowenstein PR, Coyle JT, Price DL, Kellar KJ. Nicotinic acetylcholine binding sites in Alzheimer's disease. *Brain Res* 1986;371:146–151.
14. Whitehouse PJ, Martino AM, Wagster MV, Price DL, Mayeux L, Atack JR, Kellar KJ. Reductions in [^{3}H]-nicotinic acetylcholine binding in Alzheimer's disease and Parkinson's disease: an autoradiographic study. *Neurology* 1988;38:720–723.
15. Whitehouse PJ, Martino AM, Marcus KA, Zweig RM, Singer HS, Price DL, Kellar KJ. Reductions in acetylcholine and nicotine binding in several degenerative diseases. *Arch Neurol* 1988;45:722–724.
16. Nef P, Oneyser C, Alliod C, Couturier S, Ballivet M. Genes expressed in the brain define three distinct neuronal nicotinic acetylcholine receptors. *EMBO J* 1988;7:595–601.
17. Pabreza LA, Dhawan S, Kellar KJ. [^{3}H]cytisine binding to nicotinic cholinergic receptors in brain. *Mol Pharmacol* 1991;39:9–12.
18. Clarke PB, Schwartz RD, Paul SM, Pert CB, Pert A. Nicotinic binding in rat brain: autoradiographic comparison of [^{3}H]acetylcholine, [^{3}H]nicotine and [125I]-alpha-bungarotoxin. *J Neuroscience* 1985;5:1307–1315.
19. Schulz DW, Loring RH, Aizenman E, Zigmond RE. Autoradiographic localization of putative nicotinic receptors in the rat brain using ^{125}I-neuronal bungarotoxin. *J Neurosci* 1991;11:287–297.
20. Flores CM, Rogers SW, Pabreza LA, Wolfe B, Kellar KJ. A subtype of nicotinic cholinergic receptor in rat brain is composed of alpha 4 and beta 2 subunits and is up-regulated by chronic nicotine treatment. *Mol Pharmacol* 1992;41:31–37.
21. Nybäck H, Nordberg A, Långström B, et al. Attempts to visualize nicotinic receptors in the brain of monkey and man by positron emission tomography. *Prog Brain Res* 1989;79:313–319.
22. Nordberg A, Lundqvist H, Hartvig P, Lilja A, Långström B. Kinetic analysis of regional (S)(-)^{11}C-nicotine binding in normal and Alzheimer brains–in vivo assessment using positron emission tomography. *Alzheimer Dis Assoc Disord* 1995;9:21–27.

23. Badio B, Daly JW. Epibatidine, a potent analgetic and nicotinic agonist. *Mol Pharmacol* 1994;45:563–569.
24. Houghtling RA, Davila-Garcia MI, Kellar KJ. Characterization of (±)-[^{3}H]epibatidine binding to nicotinic cholinergic receptors in rat and human brain. *Mol Pharmacol* 1995;48:280–287.
25. Perry DC, Kellar KJ. ^{3}H-epibatidine labels nicotinic receptors in rat brain: an autoradiographic study. *J Pharmacol Exp Ther* 1995;275:1030–1034.
26. London ED, Scheffel U, Kimes AS, Kellar KJ. In vivo labeling of nicotinic acetylcholine receptors in brain with [^{3}H]epibatidine. *Eur J Pharm* 1995;278:R1–R2.
27. Scheffel U, Taylor GF, Kepler JA, Carroll FI, Kuhar MJ. In vivo labeling of neuronal nicotinic acetylcholine receptors with radiolabeled isomers of norchloroepibatidine. *NeuroReport* 1995;6:2483–2488.
28. Horti AG, Ravert HT, London ED, Dannals RF. Synthesis of a radiotracer for studying nicotinic acetylcholine receptors by positron emission tomography: (±)-exo-2-(2-[^{18}F]fluoro-5-pyridyl)-7-azabicyclo[2.2.1]heptane. *J Labell Comp Radiopharm* 1996; 38:355–366.
29. Riche D, Hantraye P, Guibert B, Naquet R, Loc'h C, Maziere B, Maziere M. Anatomical atlas of the baboon's brain in the orbito-meatal plane used in experimental positron emission tomography. *Brain Res Bull* 1988;20:283–301.
30. London ED, Waller SB, Wamsley JK. Autoradiographic localization of [^{3}H]nicotine binding sites in the rat brain. *Neurosci Lett* 1985;53:179–184.
31. Nordberg A, Alafuzoff I, Winblad B. Nicotinic and muscarinic subtypes in the human brain: changes with aging and dementia. *J Neurosci Res* 1992;31:103–111.
32. Horti AG, Ravert HT, Mathews WB, Musachio JL, Kimes A, London ED, Dannals RF. Synthesis of high specific activity carbon-11 N-methylated analogs of epibatidine for imaging nAChRs [Abstract]. *J Nucl Med* 1996;37:192P.
33. Cimino M, Marini P, Fornasari D, Cattabeni F, Clementi F. Distribution of nicotinic receptors in cynomologus monkey brain and ganglia: localization of alpha 3 subunit mRNA, alpha-bungarotoxin and nicotine binding sites. *Neuroscience* 1992;51:77–86.
34. Pauly JR, Marks MJ, Gross SD, Collins AC. An autoradiographic analysis of cholinergic receptors in mouse brain after chronic nicotine treatment. *J Pharmacol Exp Ther* 1991;258:1127–1136.
35. Sullivan JP, Decker MW, Brioni JD, et al. (±)-Epibatidine elicits a diversity of in vitro and in vivo effects mediated by nicotinic acetylcholine receptors. *J Pharmacol Exp Ther* 1994;271:624–631.
36. McKay J, Lindstrom J, Loring RH. Determination of nicotinic receptor subtypes in chick retina using monoclonal antibodies and 3H-epibatidine. *Med Chem Res* 1994; 4:528–537.
37. Logan J, Fowler JS, Volkow ND, et al. Graphical analysis of reversible radioligand binding from time-activity measurements applied to [N-^{11}C-methyl]-(-)-cocaine PET studies in human subjects. *J Cereb Blood Flow Metab* 1990;10:740–747.
38. Huang SC, Barrio JR, Phelps ME. Neuroreceptor assay with positron emission tomography: equilibrium versus dynamic approaches. *J Cereb Blood Flow Metab* 1987;7:214–229.
39. Wong DF, Gjedde A, Wagner HN Jr. Quantification of neuroreceptors in the living human brain. I. Irreversible binding of ligands. *J Cereb Blood Flow Metab* 1986;6: 137–146.
40. Wong DF, Gjedde A, Wagner HN Jr, Dannals RF, Douglass KH, Links JM, Kuhar MJ. Quantification of neuroreceptors in the living human brain. II. Inhibition studies of receptor density and affinity. *J Cereb Blood Flow Metab* 1986;6:147–153.
41. Gjedde A. High- and low-affinity transport of D-glucose from blood to brain. *J Neurochem* 1981;36:1463–1471.
42. Patlak CS, Blasberg RG, Fenstermacher JD. Graphical evaluation of blood-to-brain transfer constants for multiple time uptake data. *J Cereb Blood Flow Metab* 1983;3:1–7.

Technetium-99m(V)-DMSA and Thallium-201 in Brain Tumor Imaging: Correlation with Histology and Malignant Grade

Tsuneo Hirano, Hidenori Otake, Ken Kazama, Kazuki Wakabayashi, Akira Zama, Takashi Shibasaki, Masaru Tamura and Keigo Endo

Departments of Nuclear Medicine and Neurosurgery, Gunma University, School of Medicine, Maebashi, Gunma, Japan

This study was performed to compare imaging ability between pentavalent ^{99m}Tc-DMSA and ^{201}TlCl in primary and metastatic brain tumors and to evaluate the relationship between retention and histologic malignancy. **Methods:** Patients with a brain tumor were selected by MRI and/or CT. Dynamic, early and delayed static SPECT images of the brain were obtained immediately, 30 min and 3 hr after intravenous administration of approximately 555 MBq ^{99m}Tc(V)-DMSA and 111 MBq ^{201}Tl-Cl, respectively. Both studies were performed on separate days within a week. Uptake ratios, retention ratio and retention index were calculated and compared with tumor histology and malignancy grade. **Results:** One-hundred six studies were performed on 100 patients and 118 lesions were demonstrated: 16 glioblastomas, 13 anaplastic astrocytomas (Grade III), 19 astrocytomas (Grade II), 29 meningiomas, 11 schwannomas and 14 metastases. Approximately 93% and 88%, respectively, of primary and metastatic brain tumors were demonstrated by ^{99m}Tc(V)-DMSA and ^{201}TlCl. The early uptake ratios were closely related to the tumor vascularity, but had no statistically significant difference in the tumor histology or histologic malignancy on either radiopharmaceuticals. The delayed uptake ratio, retention ratio and retention index were higher in malignant tumors than benign ones on ^{99m}Tc(V)-DMSA, however, there was no statistically significant difference between benign and malignant tumors on ^{201}TlCl. **Conclusion:** Technetium-99m(V)-DMSA washout from the tumor was highly dependent upon its histology and histologic malignancy. The delayed uptake ratio, retention ratio and retention index significantly reflected tumor histology and clearly distinguished between benign and malignant tumors with a statistically significant difference. There was no statistically significant difference in ^{201}TlCl uptake or washout among the brain tumors. Technetium-99m-DMSA is superior to ^{201}TlCl in imaging quality, sensitivity to brain tumors and specificity for differentiating benign tumors from malignant ones. These results could suggest the clinical utility of ^{99m}Tc(V)-DMSA in imaging primary and metastatic brain tumors and differentiating their histological malignancy grade noninvasively.

Key Words: technetium-99m-DMSA; thallium-201-chloride; histologic malignancy; brain tumor; retention index; SPECT

J Nucl Med 1997; 38:1741–1749

CT and MRI can demonstrate smaller lesions due to their fine spatial resolution. Furthermore, their contrast enhancement, mainly dependent upon disrupted blood brain barrier (BBB), has been used to localize the tumors, but prediction of histopathological diagnosis was very difficult. Thallium-201-chloride, one of the most widely used radiopharmaceuticals, has been reported to differentiate, to some extent, benign lesions from malignant lesions of the lung (*1*), thyroid gland (*2*) and brain tumors (*3–7*), depending upon the uptake ratio and prolonged washout phase of radiotracer from the tumor tissue (*5–7*).

Pentavalent ^{99m}Tc(V)-DMSA was developed for a tumor imaging agent (*8,9*) and its accumulation has been reported in

Received Sep. 10, 1996; revision accepted Feb. 28, 1997.
For correspondence or reprints contact: Tsuneo Hirano, MD, 3-13-5 Showa-machi, Maebashi, Gunma 00371, Japan.